Articles

Molecular Organization in Striated Domains Induced by Transmembrane α-Helical Peptides in Dipalmitoyl Phosphatidylcholine Bilayers[†]

Emma Sparr,*,[‡] Dragomir N. Ganchev,[‡,§] Margot M. E. Snel,[§] Anja N. J. A. Ridder,[‡] Loes M. J. Kroon-Batenburg,[∥] Vladimir Chupin,[‡] Dirk T. S. Rijkers,[⊥] J. Antoinette Killian,[‡] and Ben de Kruijff[‡]

Department of Biochemistry of Membranes, Institute of Biomembranes, Utrecht University, Padualaan 8, NL-3584 CH Utrecht, The Netherlands, Department of Physical Chemistry of Interfaces, Faculty of Chemistry, Utrecht University, Padualaan 8, NL-3584 CH Utrecht, The Netherlands, Department of Crystal and Structural Chemistry, Utrecht University, Padualaan 8, NL-3584 CH Utrecht, The Netherlands, and Department of Medicinal Chemistry, Faculty of Pharmaceutical Sciences, Utrecht University, Padualaan 8, NL-3584 CH Utrecht, The Netherlands

ABSTRACT: Transmembrane (TM) α-helical peptides with neutral flanking residues such as tryptophan form highly ordered striated domains when incorporated in gel-state 1,2-dipalmitoyl-*sn*-glycero-3-phosphocholine (DPPC) bilayers and inspected by atomic force microscopy (AFM) (*1*). In this study, we analyze the molecular organization of these striated domains using AFM, photo-cross-linking, fluorescence spectroscopy, nuclear magnetic resonance (NMR), and X-ray diffraction techniques on different functionalized TM peptides. The results demonstrate that the striated domains consist of linear arrays of single TM peptides with a dominantly antiparallel organization in which the peptides interact with each other and with lipids. The peptide arrays are regularly spaced by ±8.5 nm and are separated by somewhat perturbed gel-state lipids with hexagonally organized acyl chains, which have lost their tilt. This system provides an example of how domains of peptides and lipids can be formed in membranes as a result of a combination of specific peptide−peptide and peptide−lipid interactions.

The biological membrane is a highly complex molecular system consisting of a variety of protein and lipid species, and its molecular organization is believed to be important for different biological functions. One important aspect of this is the spatial segregation of lipids and proteins in domains of different composition. This is exemplified in the so-called raft model, which considers small size domains as membrane lipid rafts that serve as platforms for lipid and protein transport or as relay stations in intracellular signaling (*2*). In recent years, considerable research has been directed toward the physical origin and the biological function of domain formation (*3−5*). The majority of these studies concern domain formation because of segregation of the different lipid components. Partitioning of membrane proteins between the different phases may further affect domain formation, and this may serve as a mechanism for membrane sorting. It is also possible that domains can be induced by the presence of proteins in a lipid bilayer that is not by itself segregating. For instance, it has been shown by atomic force microscopy (AFM) that different transmembrane (TM) proteins and peptides can form domains of line-type peptide aggregates in gel-state PC model membranes, as exemplified by the lung surfactant protein C (SP−C) and gramicidin A (*6*, *7*). The formation of line-type aggregates appears to be a more general property of TM peptides. In recent AFM studies, we established that the so-called WALP peptides induce the formation of highly characteristic striated domains and line-type depressions in a gel-state 1,2-dipalmitoyl-*sn*-glycero-3-phosphocholine (DPPC) bilayer (*1*). These latter peptides are designed to mimic TM segments of integral membrane proteins, having a hydrophobic core of alternating leucines and alanines, flanked on both ends by two tryptophan residues. WALP peptides were shown to adopt TM α-helices in a variety of lipid bilayers, where the tryptophan residues preferentially reside in the interfacial region of the bilayer (*8*). The pattern of the striated domains induced by these peptides consists of line-type depressions and elevations, equally spaced with a repeat distance of approximately 8 nm (*1*). When the lipid/peptide ratio is varied, the size of the domains changes, although their morphology is unaltered; therefore, at a 8:1 lipid/peptide molar ratio, the entire bilayer consists of striated domains. At low peptide concentrations the domains are interconnected by line-type depressions in the bilayer. The striated domains were observed by AFM in

* To whom correspondence should be addressed: Physical Chemistry 1, Center for Chemistry and Chemical Engineering, Lund University, P. O. Box 124, SE-221 00 Lund, Sweden. Telephone: +46 (0)46 222 48 12. Fax: +46 (0)46 222 44 13. E-mail: emma.sparr@fkem1.lu.se.
[‡] Department of Biochemistry of Membranes.
[§] Department of Physical Chemistry of Interfaces.
[∥] Department of Crystal and Structural Chemistry.
[⊥] Department of Medicinal Chemistry.

supported bilayers but could also be visualized by electron microscopy (EM) in vesicle dispersions (*9*), demonstrating that the aggregation of these peptides is not determined from the properties of the negatively charged mica. Striated domains are also induced by similar peptides with other neutral helix-flanking residues, but not for peptides carrying charged anchoring residues (*9*).

On the basis of the AFM data, a model for the molecular organization of the striated domains was presented (*1*). However, actual information on the molecular architecture of the domains was still lacking, and this forms the goal of the present study. We analyzed the striated domains in the following ways: by localizing the peptides using AFM in combination with decoration with gold particles, by analyzing the peptide surroundings by photocross-linking and fluorescence spectroscopy, and by studying lipid organization using ^{2}H-NMR on deuterated lipids and X-ray diffraction. For these studies, the WALP23 peptides were functionalized with different probes. The combination of these results provides a detailed picture of the molecular organization and interactions in this system and thereby brings insight into the mechanisms behind the formation of the highly ordered peptide-rich domains.

MATERIALS AND METHODS

Materials. DPPC was obtained from Avanti Polar Lipids (Alabaster, AL), and acyl chain perdeuterated DPPC-d_{62} was obtained from Cambridge Isotope Laboratories Inc. (Andover, MA). MilliQ water was used for all experiments.

The peptides Ac-GWW(LA)$_8$LWWA-NH$_2$ (Ac-WALP23), Ac-CGWW(LA)$_8$LWWA-NH$_2$ (Cys$_N$-WALP23), Ac-GWW-(LA)$_8$LWWC-NH$_2$ (Cys$_C$-WALP23), and SATA-GWW(LA)$_8$-LWWA-NH$_2$ (SATA-WALP23) were synthesized automatically on an Applied Biosystems 433A Peptide Synthesizer using the FastMoc protocol (*10*) on a 0.25 mmol scale. The latter peptide was end-capped with *S*-acetyl-thioglycolic acid using its corresponding pentafluorophenyl active ester in the absence of any base to avoid premature cleavage of the thioester. Peptide synthesis was carried out on ArgoGel Rink-Amide resin to obtain C-terminal amides. N^α-9-fluorenyl-methyloxycarbonyl (Fmoc)-protected amino acids with the side chain of tryptophan protected by tertbutyloxycarbonyl (Boc) (*11*) and the cysteine side chain protected by a trityl (Trt) group were used. Coupling of N^α-Fmoc amino acids (1 mmol, 4 equiv) were performed with 2-(1*H*-benzotriazol-1-yl)-1,1,3,3-tetramethyluronium hexafluorophosphate/*N*-hydroxybenzotriazole (HBTU/HOBt) (*12*) in the presence of 8 equiv *N*,*N*-diisopropylethylamine (DIPEA) in *N*-methylpyrrolidone (NMP) for 45 min. Fmoc removal was carried out with 20% piperidine in NMP for 70 s. Any remaining amino groups after incomplete coupling were acetylated by acetic anhydride/DIPEA/HOBt in NMP. After removal of the final Fmoc group, the resin was extensively washed with NMP and dichloromethane, and subsequently, the peptide resin was dried in a vacuum desiccator.

The peptides were cleaved from the resin and deprotected by treatment with trifluoroacetic acid/H$_2$O/triisopropylsilane 95:2.5:2.5 (v/v/v) at room temperature for 3 h. The peptides were precipitated at $-20\ °$C with methyl tertbutyl ether/hexane 1:1 (v/v). The precipitates were decanted and subsequently washed with cold methyl tertbutyl ether/hexane

1:1 (v/v) (3 times) and finally lyophilized from tert-BuOH/H$_2$O 1:1 (v/v).

Preparation of SH-WALP23. SH-WALP23 was prepared according to the following procedure. SATA-WALP23 (20 mg) was dissolved in 1,4-dioxane (2800 μL) and methanol (1000 μL), and 4 M NaOH (200 μL) was added in one portion. The obtained reaction mixture was stirred for 2 min after which 2 N HCl (400 μL) was added. Subsequently, the reaction mixture was evaporated in vacuo, resolubilized in CH$_3$CN/H$_2$O 1:1 (v/v), and lyophilized to yield the thioglycolic acid WALP23 peptide with a free sulfhydryl functionality at the N-terminus (SH-WALP23).

Preparation of Pyrene-Labeled WALP23. In a typical conjugation experiment, 10 μmol of peptide with a free thiol functionality (Cys$_N$-WALP23 or Cys$_C$-WALP23) was dissolved in 2,2,2-trifluoroethanol (TFE, 2.5 mL) and the clear solution was purged with dry N$_2$ for 5 min. Then, 10 μL of triethylamine was added to obtain a pH between 8.5 and 9, which was followed by the addition of 12.5 μmol of pyrene—maleimide [Molecular Probes Europe BV (Leiden, The Netherlands)] conjugate, which was dissolved in N$_2$-purged TFE (1 mL), and the obtained reaction mixture was gently stirred for 48 h in the dark at 4 $°$C. Finally, the peptide—pyrene conjugate was precipitated with cold methyl tertbutyl ether/hexane 1:1 (v/v), and the precipitate was decanted and subsequently lyophilized from tert-BuOH/H$_2$O 1:1 (v/v).

Ac-GWW(LA)$_2$F(TMD)A(LA)$_5$LWWA-NH$_2$ (TMD-WALP23) was synthesized as described earlier (*13*).

Peptide purity was analyzed by analytical high-performance liquid chromatography (HPLC) on a Merck LiChroSpher CN column, with a 5 μm particle size and a 100 Å pore size (length = 250 mm, and inside diameter = 4.6 mm) at a flow rate of 1.0 mL/min using a linear gradient of buffer B (100% in 20 min) from 100% buffer A [buffer A = 0.1% TFA in H$_2$O, and buffer B = 0.1% TFA in CH$_3$CN/H$_2$O 95:5 (v/v)]. A second HPLC analysis was run on an Alltech Adsorbosphere XL column, with a 5 μm particle size and a 300 Å pore size (length = 250 mm, and inside diamter = 4.6 mm) at a flow rate of 0.75 mL/min using a linear gradient of buffer B (100% in 60 min) from 90% buffer A [buffer A = 50 mM triethylamine/H$_3$PO$_4$ at pH 2.25 in H$_2$O/CH$_3$CN 8:2 (v/v), and buffer B = 50 mM triethylamine/H$_3$PO$_4$ at pH 2.25 in H$_2$O/CH$_3$CN/isopropyl alcohol 5:50:45 (v/v/v)]. Purity was determined to be 95% or higher. The peptides were characterized by matrix-assisted laser desorption ionization—time-of-flight (MALDI—TOF) analysis, which was performed on a Kratos Axima CFR apparatus, with ACTH-(18-39) as the external reference and α-cyano-4-hydroxycinnamic acid as the matrix.

The amino acid sequences for the peptides used for further experiments are given in Table 1.

Preparation of Supported Bilayers. Supported bilayers on mica of DPPC and the desired amount of WALP peptide were prepared via vesicle fusion essentially as described before (*1*, *7*), except that the 20 mM NaCl solution used for sample preparation contained 0.05 mM dithiothreitol (DTT) to prevent oxidation of SH-WALP23.

AFM Imaging. The supported bilayers were covered by the NaCl solution during the measurements. The samples were scanned in contact mode, using oxide sharpened Si$_3$N$_4$ tips attached to a triangular cantilever with a spring constant of 0.06 N/m (NanoProbe, DI, Santa Barbara, CA). All images

Table 1: Structures of Peptides Used, Including Nomenclature

peptide	amino acid sequence
Ac-WALP23	Ac-Gly-[Trp]$_2$-[Leu-Ala]$_8$-Leu-[Trp]$_2$-Ala-NH$_2$
SH-WALP23	SH-CH$_2$-CO-Gly-[Trp]$_2$-[Leu-Ala]$_8$-Leu-[Trp]$_2$-Ala-NH$_2$
TMD-WALP23	Ac-Gly-[Trp]$_2$-[Leu-Ala]$_2$-Phe(TMD)-Ala-[Leu-Ala]$_5$-Leu-[Trp]$_2$-Ala-NH$_2$
Pyr$_N$-WALP23	Ac-Cys(pyrene)-Gly-[Trp]$_2$-[Leu-Ala]$_8$-Leu-[Trp]$_2$-Ala-NH$_2$
Pyr$_C$-WALP23	Ac-Gly-[Trp]$_2$-[Leu-Ala]$_8$-Leu-[Trp]$_2$-Gly-Cys(pyrene)-NH$_2$

were recorded at temperatures between 23 and 28 °C at a minimal force (100−200 pN) as described before (*1*), using a Nanoscope III AFM (Digital Instruments, Santa Barbara, CA).

Decoration of Bilayers with Gold Particles. A suspension of colloidal gold particles was prepared using the method of Duff et al. (*14*). The size of the gold particles was found to be 13 nm as measured by dynamic light scattering (Zeta-sizer 3000, Malvern Instruments, U.K.). Dynamic light scattering was also used to confirm that the thio group of SH-WALP23 in DPPC vesicles was accessible to the gold particles as they caused massive vesicle aggregation (not shown). After visualization of the bilayer with the striated domains, the AFM head was removed and 10 μL of gold particle suspension was added to the NaCl/DTT solution covering the sample. After 10 min, the sample was rinsed 3 times with 75 μL of the NaCl/DTT solution to remove unbound gold particles. Then, the AFM head was mounted again, and the labeled sample was imaged.

Sample Preparation. For all other measurements, WALP-containing multilamellar DPPC vesicles (MLVs) were used. The vesicles were prepared from dry mixed peptide−lipid films of desired composition as described before (*15*). The mixed film was hydrated with the desired solution and dispersed by vigorous vortexing at 50 °C, and the samples were subjected to 10 cycles of freeze−thawing. The resulting multilamellar vesicles were stored at 4 °C until use. For the samples used in photocross-linking studies, these procedures were carried out in the dark as much as possible (*13*).

Photocross-linking. Photocross-linking of 3-(trifluoro-methyl-3H-diazirin-3-yl)phenylalanine (TMD-phenylalanine) containing WALP23 was carried out at room temperature in MLV of DPPC in 0.5 mL of 20 mM ammonium acetate at pH 7.5 (final lipid concentration of 1.88 mM) with lipid/peptide ratios between 8:1 and 25:1. After cross-linking, the samples were analyzed by SDS−PAGE essentially as described in refs *16* and *17*.

Fluorescence Spectroscopy. Fluorescence experiments were performed on MLV with lipid/peptide ratios between 8:1 and 1000:1 in water (or with similar results in 20 mM NaCl) at a final peptide concentration of 0.25 μM. The samples (1.2 mL) were continuously stirred and temperature controlled in a 10 mm quartz cuvette and analyzed on a SLM-Aminco SPF-500 C fluorimeter. The fluorescence of pyrene was analyzed between 370 and 600 nm (bandwidth of 5 nm) and at an excitation wavelength of 350 nm (bandwidth of 5 nm). The absorbance of each sample was measured at the excitation and emission wavelength on a Perkin−Elmer UV−vis Lambda 18 spectrometer. These data were used to calculate the inner-filter effect as described in ref *18*.

NMR Spectroscopy. ^{2}H-NMR spectra of DPPC-d_{62} MLVs in deuterium-depleted water, with and without peptide, were recorded and processed on a Bruker Avance 500 WB spectrometer as described before (*19, 20*).

X-ray Diffraction. The lipid suspensions, with or without peptide, were inserted in a 0.5 mm Boron glass capillary and were sealed with wax to prevent drying. They were mounted on a goniometer head in a horizontal position perpendicular to the X-ray beam. The Cu K$_\alpha$ radiation was produced by a rotating anode at 45 kV and 40 mA on a Nonius FR591 generator, using osmic mirrors. Images were recorded by a Mar345dtb image plate using a 0.15 mm pixel size, positioned at 250 mm from the sample and were integrated during 300 min. Scattering by air was recorded separately and subtracted from the scattering of the samples.

The images were analyzed by VIW that is part of the EVAL14 software suite (*21*). The X-ray data sometimes show preferred orientation of the lamellar ordering, which helps in the assignment of the *d* spacings. In all cases, average radial profiles of the diffraction patterns were made, giving the scattered intensity versus the Bragg angle 2θ. The small angle scattering was limited to ∼70 Å because of the beam stop.

Analytical Methods. The peptide concentration in the stock solution was determined from the absorbance at 280 nm using an extinction coefficient of 22 400 M^{-1} cm^{-1}. Phospholipids were quantified according to Rouser et al. (*22*). Nanoflow electrospray ionization−mass spectrometry (ESI−MS) measurements were performed as described (*13*).

RESULTS

AFM Imaging of Striated Domains and Localization of Peptide. In this study, a number of different WALP-23 analogues were used (Table 1). To test whether these peptides still had the ability to form striated domains and line-type depressions, the peptides were incorporated into supported DPPC bilayers and inspected by AFM. Very similar morphologies were observed in all systems. An example for DPPC/SH-WALP23 at a molar ratio of 50:1 is shown in Figure 1A. Next to smooth areas corresponding to the gel-state bilayer of DPPC, striated domains consisting of regularly spaced dark (thinner) lines separated by lighter (thicker) lines are present that are connected with line-type depressions (dark). The repeat distance between the dark lines within the domains was similar for all peptides and was found to be 8.5 ± 1 nm. We conclude that all WALP peptides used in this study form comparable striated domains. Small variations in the morphology of the domains (domain size and curvature of the stripes) were observed for the different peptides. This demonstrates that the precise morphology depends in a subtle manner on the precise chemical nature of the peptides, as has also been observed for striated domains of WALP peptides of different helix length and flanking residues (*9*).
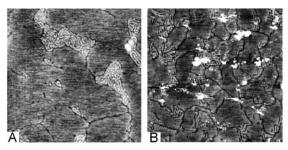
FIGURE 1: AFM images of striated domains of supported bilayers of WALP and DPPC at a lipid/peptide ratio of 50:1. (A) SH-WALP23. (B) DPPC/SH-WALP23 bilayer after addition of gold particles. The 13 nm gold particles are visualized as light dots. Temperature, 24 ± 2 °C; image size, 500 × 500 nm; Z scale, 3 nm.

The location of SH-WALP23 in the sample was probed by decoration of the supported bilayer with 13-nm-sized gold particles (Figure 1B). The nanoparticles show up as light dots on the bilayer and are localized primarily on the striated domains. Analysis of more than 200 particles counted on 9 different samples showed that 79% of them were localized on striated domains, 14% were present on the line type depressions, and 7% was detected on the flat bilayer. When the experiment was carried out with the control Ac-WALP23 peptide, which does not contain a free SH group, no particles were observed on the bilayer (data not shown). From these results, we conclude that WALP is localized in the striated domains and line-type depressions. Probing the striated domains of SH-WALP23 with a gold-covered AFM tip confirmed this conclusion (Ganchev, D. et al., unpublished observations).

Chemical Surrounding of WALP in the Striated Domains. To inspect the surroundings of WALP in the striated domains containing bilayers, a WALP23 analogue was prepared containing a photoactivatable TMD-phenylalanine at position 6 in the hydrophobic core (Table 1). The TMD-WALP23 was incorporated at a DPPC/peptide ratio of 8:1, under which the condition of the entire bilayer of WALP-DPPC consists of striated domains (*1*). Illumination causes formation of a very reactive carbene that immediately inserts even into chemically inert CH-bonds (*23*), thus forming covalent complexes with neighboring molecules. After irradiation with UV light for different time periods, samples were analyzed on SDS−PAGE using SDS−tricine gel electrophoresis (*16*). In the absence of photoactivation (lane $t = 0$ of Figure 2A), two bands are observed beside the bands corresponding to the pure monomeric TMD-WALP23 and the pure lipid, which is blue because of staining with Coomassie Blue. Upon illumination, two new bands are observed (lanes $t = 5$ and 10 of Figure 2A). First, a prominent new blue band is observed, which runs slightly higher than WALP. This is indicative for a cross link to DPPC, which was confirmed by ESI−MS (not shown). Similar bands were observed for dilute samples of TMD-WALP23 in bilayers of unsaturated PCs (*13*). The next new band runs at a molecular weight of around 3.5 kD. This band is already present in small quantities prior to illumination, but increases in intensity upon illumination. We failed to unambiguously identify this band by mass spectrometry, but we assume it corresponds to a dimer of TMD-WALP23 because of its molecular weight and because it runs at exactly the same height as a dimer that we prepared by oxidation of SH-WALP23 (not shown).
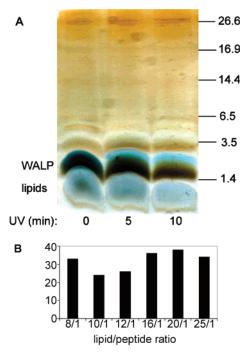

FIGURE 2: Photocross-linking of TMD-WALP23 in gel-state DPPC bilayers. (A) TMD-WALP23 reconstituted in DPPC vesicles at a lipid/peptide ratio of 8:1 and irradiated with UV light for the indicated times. The samples were analyzed by SDS−PAGE, and the position and molecular weights of marker proteins are shown. (B) Relation between the amount of peptide dimer and the lipid/peptide ratio. The amount of dimers is given as the percentage of the total amount of peptide detected on the gel. Samples were irradiated for 10 min.

Quantification of the intensity of the putative dimer band over a range of lipid/peptide ratios shows that it amounts to about 30% of the total peptide content and that it is nearly independent of the lipid/peptide ratio (Figure 2B). These results strongly suggest that, within the striated domains, a constant and specific chemical environment is present in which the peptide interacts with both DPPC and neighboring peptide molecules.

Peptide Association and Topology. To get further evidence for the occurrence of direct peptide−peptide interactions within the striated domains, we studied WALP peptides that were labeled with a pyrene group either at the N-terminus (Pyr$_N$-WALP23) or C-terminus (Pyr$_C$-WALP23) (Table 1). Within this assay, it is possible to distinguish between parallel and antiparallel orientations of adjacent peptides. When two pyrenes are within close proximity, an excimer fluorescence signal is observed. Interactions between antiparallel helices can therefore only be detected when both types of peptides are present, while parallel helix−helix interactions can also be detected for samples that contain only one type of peptide. Figure 3A compares the pyrene fluorescence emission spectra for samples of DPPC/peptide, with a molar ratio of 25:1, where, in one case, the sample contains only the peptide that is labeled at the N-terminus and, in the other case, a 1:1 mixture of Pyr$_N$-WALP23 and Pyr$_C$-WALP23 is present. At this peptide concentration, striated domains are present. In both cases, the spectra show the characteristic pyrene monomer peaks at wavelengths between 375 and 420 nm and an excimer fluorescence at 490 nm, directly demonstrating the occurrence of peptide−peptide interactions. Interestingly, the excimer fluorescence of the sample containing both
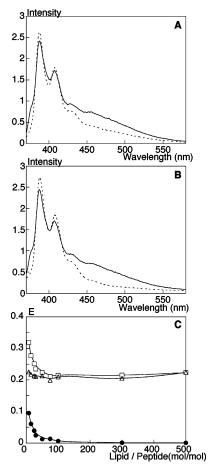
FIGURE 3: Fluorescence data for pyrene-labeled WALP23 in DPPC bilayers at 22 °C. (A) Fluorescence spectra for the Pyr_N-WALP23 (- - -) and the equimolar mixture Pyr_N-WALP/Pyr_C-WALP23 (—) in DPPC vesicles, with a lipid/peptide ratio of 25:1. (B) Fluorescence spectra for the Pyr_N-WALP23 (- - -) and the equimolar mixture Pyr_N-WALP23/Pyr_C-WALP23 (—) in DPPC vesicles, with a lipid/peptide ratio of 500:1. (C) Quantification of the excimer intensity (E) as a function of the lipid/peptide ratio; experimental data for the parallel interactions, $E_{parallel}$, from samples including Pyr_N-WALP23 (●), parallel and antiparallel interactions, $E_{parallel+antiparallel}$, from samples including equimolar mixture Pyr_N-WALP23/Pyr_C-WALP23 (□), and calculated values for antiparallel interactions, $E_{antiparallel}$ (△), where $E_{antiparallel} = E_{parallel+antiparallel} - E_{parallel}$. The excimer intensity was obtained from the intensity of the excimer emission peak (490 nm). To facilitate the comparison in C, the excimer intensity was further corrected for the background intensity at the same wavelength (obtained from samples only showing monomer fluorescence) by simple subtraction.

N- and C-terminal-labeled peptides is substantially higher than the case where only an N-terminal pyrene is present. This strongly suggests a preference for antiparallel orientations of the peptides in the striated domains. At lower peptide concentrations, striated domains are not formed and the peptides are only present in line-type depressions. In these situations, excimer formation is only detected when both types of peptides are present, as illustrated in Figure 3B for a lipid/peptide ratio of 500:1. The combined results in Figure 3B therefore suggest that the line-type depressions consist of single lines of peptides with alternating orientation.

The fluorescence characteristics of these two peptide systems were analyzed over a large range of lipid−peptide concentrations, and the observed excimer fluorescence intensity is shown in Figure 3C. It is evident that the excimer intensity is substantially higher for the mixtures of Pyr_N-
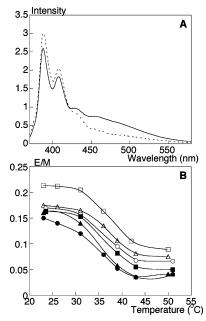

FIGURE 4: Fluorescence data for pyrene-labeled WALP23 in DPPC bilayers at different temperatures. (A) Fluorescence spectra for an equimolar mixture of Pyr_N-WALP23/Pyr_C-WALP23 at 22 °C (—) and 50 °C (- - -). Lipid/peptide ratio of 50:1. (B) Quantification of the excimer/monomer ratio (E/M) as a function of the concentration at lipid/peptide ratios of 8:1 (□), 25:1 (△), 30:1 (○), 50:1 (■), 100:1 (▲), and 500:1 (●).

WALP23 and Pyr_C-WALP23 than for the Pyr_N-WALP23 alone. This indicates that, in the gel-state bilayers, an antiparallel close association of the peptide occurs and it is preferred over a parallel association. Excimer formation strongly increases below lipid/peptide ratios of 100:1, which is the concentration where striated domains start to become visible (*1*). This increase in excimer fluorescence appears to originate from an increase in parallel interactions (Figure 3C), while the preferred antiparallel orientation is approximately constant over the entire concentration range. We can therefore conclude that the degree of antiparallel interaction is the same whether the peptides are present in line-type depressions or striated domains.

When the samples are heated to 50 °C, which is above the phase-transition temperature of pure DPPC (41 °C), the excimer fluorescence at 490 nm for the equimolar Pyr_N-WALP23/Pyr_C-WALP23 mixtures sharply drops. Similar effects are observed at high peptide concentrations (Figure 4A), when striated domains occur, and at low peptide concentrations (not shown), when the peptides are only present in line-type depressions. The complete temperature dependence of the excimer intensity, represented as the excimer/monomer ratio, is shown in Figure 4B for samples with different peptide concentrations. The data clearly demonstrate that the excimer intensity decreases upon heating over the 30−42 °C temperature interval, suggesting that melting of the domains occurs and, thereby, a reduction of the extent of lateral peptide−peptide association. The broadness of the transition and its independence of the lipid/peptide ratio suggest that, in all cases, the peptides see a similar lipid environment, which has slightly different properties than the pure DPPC bilayer. To get a better understanding of the organization and dynamics of the lipids in the striated domains, ^{2}H-NMR was employed using chain-perdeuterated DPPC.
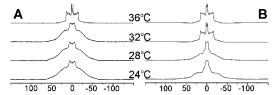
FIGURE 5: ^{2}H-NMR spectra recorded at different temperatures of aqueous dispersions of (A) DPPC-d_{62} and (B) DPPC-d_{62} containing WALP23 at a lipid/peptide molar ratio of 8:1.

Lipid Order and Dynamics. The ^{2}H-NMR spectra of pure DPPC and a DPPC/WALP23 (8/1) sample, recorded at different temperatures, are shown in Figure 5. The spectra of pure chain-deuterated DPPC at 36 °C (Figure 5A) are typical for the liquid crystalline bilayer in which the acyl chains are melted. Note that full chain deuteration causes a decrease in chain melting by 5 °C (*24*). At lower temperatures, spectra broaden and show the typical features of immobilized gel-state acyl chains. The spectra of the peptide-containing samples in the liquid crystalline state are very similar to those of the DPPC sample. In both cases, spectral broadening is observed upon lowering the temperature, which is typical of chain immobilization in the gel state. However, at the lower temperatures, two differences can be noticed in the spectra of the peptide-containing sample as compared to spectra for the pure DPPC. First, the phase transition appears broadened and occurs at lower temperatures, which is consistent with the pyrene fluorescence data shown in Figure 4C. Second, although spectral broadening occurs at low temperatures (24 °C), the spectra obtained from the peptide-containing sample remain different from that of the pure DPPC, suggesting a somewhat altered acyl chain order and/or dynamics in the striated domains.

The organization of the striated domains was further investigated by means of X-ray diffraction. Figure 6 shows the diffraction patterns of the same samples that were used in the ^{2}H-NMR experiment shown in Figure 5. At larger diffraction angles, the prominent 4.22 Å reflection typical of gel-state hexagonally packed acyl chains shows up in both samples. This directly demonstrates that the lipids in the striated domains are closely packed, as in the gel state. However, the diffraction peak of DPPC in the striated domains is slightly broader than for pure DPPC, suggesting a slightly reduced acyl chain order, which is consistent with the ^{2}H-NMR results.

Figure 6 also shows the occurrence of at least 5 orders of Bragg peaks for the lamellar phases, thus providing accurate measurements of the lamellar repeat distance. The increase in lattice spacing from 64 to 70 Å in the presence of the peptides agrees nicely with an increased thickness of the lipid bilayer between the peptide stripes in the striated domains and is most likely due to a reduction in the tilt of the lipids in the striated domains compared to the pure DPPC L$_{\beta'}$ gel phase. The change in tilt angle can be estimated to be 26°, assuming the same degree of swelling in both lipids. This value is close to the chain tilt angle of 32 ± 0.5° reported for DPPC in the L$_{\beta'}$ gel phase (*25*). We can therefore conclude that the lipid acyl chains are almost nontilted when present in the peptide-rich striated domains.

The diffraction pattern of the peptide-containing sample shows an additional peak corresponding to a repeat distance of 10.4 Å. We noticed that the samples became oriented in
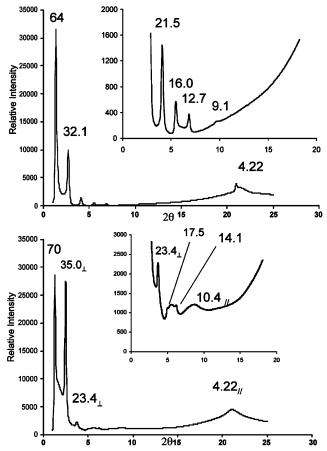

FIGURE 6: X-ray diffraction pattern recorded at 19 °C for (A) DPPC and (B) DPPC in striated domains.

the capillary and the extent of orientation could be improved by reduction of the excess water in the system by drying the sample in air (not shown). This provides us with a means to establish the spatial relation between the orientations of the diffraction lattices. From the X-ray diffraction patterns, we can conclude that the lattice giving rise to a 10.4 Å reflection runs parallel to the lattice of the 4.22 Å reflections, which corresponds to the nontilted acyl chains but is perpendicular to the reflections corresponding to the lamellar repetition. On the basis of this and on the occurrence of peptide−peptide interactions, we interpret this peak as the separation between adjacent α-helical peptides. The value of 10.4 Å is in good agreement with the predicted distance between TM α-helices (*26*).

DISCUSSION

The aim of this study is to gain insight into the molecular organization of the highly ordered striated domains induced by TM α-helical peptides, like WALP, in DPPC bilayers under gel-state conditions. We investigated the striated domains with a broad range of techniques, addressing both the molecular organization of the peptides and lipids, as well as overall bilayer organization. The results lead to a detailed model of the molecular organization of striated domains and to insight into the mechanism of formation, which will be presented after we discuss the conclusions drawn from the various experimental approaches.

Peptide−Peptide Interactions in Striated Domains. From the AFM studies, we can localize the peptides to the striated domains and line-type depressions. We can further conclude

that these structures only form when the lipids are in the gel state. One explanation for this might lie in the low solubility of the peptides in the tightly packed bilayer, where the peptides are simply "squeezed out" from the bilayer to accumulate in the boundaries between lipid domains of different tilting directions (*27*) in a way analogous to the surface enrichments of contaminants in a crystal. However, this cannot explain why the segregated system forms highly ordered domains rather than irregular clusters of the insoluble peptides.

One important conclusion in the present study is that the peptides form 1D aggregates that appear as single-line peptides, in which the peptides are arranged in an alternating manner to almost exclusively form antiparallel contacts. A plausible explanation for such an antiparallel orientation lies in the observation that the peptide α-helices have a macro-dipole moment with a positive half-unit charge at the N-terminal end of the helix and a compensatory negative charge at the C-terminal end (*28*). Within the 1D aggregates, peptide−peptide and peptide−lipid interactions occur as demonstrated by cross-linking experiments.

The distance between the peptides in the striated domains is determined from the X-ray diffraction data to 10.4 Å. Furthermore, it is shown in the fluorescence experiments that interactions between antiparallel peptides are constant over the whole range of lipid/peptide ratios from 8:1 to 1000:1. The peptide−peptide interactions therefore seem to be the same in the single lines in the line-type depressions and within the stripes in the domains. The line-type depressions can be seen as precursors for the striated domains, in which the 1D peptide aggregates accumulate and self-organize in a highly ordered structure. In addition to the antiparallel interactions, interactions between parallel peptides are also detected in the striated domains. The parallel interactions might arise because of the intersections between different stripes in the highly concentrated striated domains (Figure 7A), implying that more than two peptides are in contact with each other.

The pattern of the striated domains induced by WALP23 resembles to some extent the ripple gel phases (*29, 30*). However, it was previously concluded that the striated domains do not correspond to this phase because the repeat distance remains constant upon changing the length of the peptides or lipids (*1, 9*) or to any other modulated phase (*31*). Moreover, the striated domains were distinctly different from the rippled phase that could be simultaneously observed by AFM in multilayered parts of the preparation (*9*). Furthermore, striated domains are also observed when WALP peptides are incorporated in sphingomyelin bilayers, which unlike DPPC, do not form a ripple gel phase (Ganchev. D., unpublished observation).

Lipid−Peptide Interactions in Striated Domains. The packing of the lipids in the bilayer and their interactions with the peptides are also bound to play an important role in the formation of the specific structures in the striated domains. The ^{2}H-NMR and X-ray diffraction studies show that the hexagonal packing of the gel-state lipids is also retained at very high peptide concentrations, while there are some alterations in the molecular packing and motion. The lipids loose their tilt when present in the striated domains, as shown from the thickening of the bilayer. These changes are most likely explained by unfavorable interactions between the
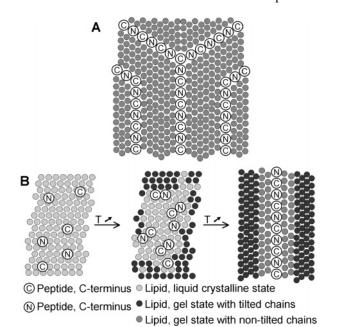

FIGURE 7: Schematic representations for (A) the proposed organization of 1D arrays of peptides with antiparallel orientation in striated domains and (B) the proposed mechanism for formation of these 1D arrays when the sample is cooled from a liquid crystalline to a gel-state bilayer.

tilted lipid acyl chains and the outer surface of the single lines of peptides. However, the lipids in direct contact with the peptide are most likely somewhat distorted because of the extensive mismatch in length of a gel-state bilayer with nontilted chains and the length of the hydrophobic part of the WALP23 helix, as proposed in ref *1*.

The fluorescence and NMR studies also demonstrate interplay between the lipid phase behavior and peptide aggregation. First, aggregation of peptides is only observed at temperatures when the lipids are in the gel state. In the liquid crystalline bilayer, the peptides seem to spread out in the bilayer to primarily be surrounded by lipids. Second, the chain-melting temperature of the lipids is lowered by the presence of peptides. The NMR data show that the chain-melting temperature is about 5 °C lower for the lipids in the striated domains compared to the pure DPPC. This result can be compared to a recent DSC (differential scanning calorimetry) study of DPPC/WALP23, where an anomalous transition was detected at 38 °C at a lipid/peptide ratio of 25:1, besides the main transition at 41.6 °C (*32*). In light of the present study, we propose that the additional transition corresponds to the melting of the striated domains that are coexisting with the DPPC bilayer. The broad transition observed in the fluorescence studies (Figure 4B) likely includes both the melting of the DPPC bilayer and the melting of the lipids in the striated domains.

Peptide−Peptide and Lipid−Peptide Interactions in the Formation of Striated Domains. The stripes of peptides observed in striated domains and line-type depressions are up to 500 nm long (*1*), which corresponds to at least 350 peptide molecules. Our results indicate that the peptides within these lines have an alternating orientation. In the sample preparation, the lipid vesicles are cooled from high temperature, implying a phase transition of DPPC from liquid crystalline to gel-state bilayers. We propose that, during the phase transition, the peptides accumulate in liquid

crystalline domains and are excluded from coexisting gel-phase domains (Figure 7B). Recently, using the same fluorescence approach, we observed formation of antiparallel dimers in liquid crystalline bilayers at high peptide contents (Sparr, E. et al., unpublished observations). Similar behavior has also been proposed for the unflanked TM Ac-(LA-LAAAA)$_3$-Am analogue peptides (*33*). We therefore suggest that antiparallel dimers are already formed before the complete bilayer is in the gel phase and that these dimers then aggregate into 1D arrays at temperatures where the gel phase covers the whole bilayer.

At the next level, these 1D aggregates form highly ordered striated domains. The structure of these domains indicates a delicate balance between lipid−peptide and peptide−peptide interactions, where the presence of aggregates of the TM peptide influences the tilt angle and motion of the surrounding lipids. The interaction of the lipids with the peptide aggregate would likely affect a few layers of lipids, and this might be reflected as a constant width of ±8.5 nm of the lipid regions separating two peptide stripes. The hexagonal packing of the gel-state lipids may also be reflected in the arrangement of the 1D peptide arrays, which can explain the hexagonal organization of peptide stripes within the domains (*1*). In conclusion, the formation of highly ordered striated domains arise because of a delicate balance between peptide−peptide interactions (antiparallel orientation within 1D aggregates), lipid−peptide interactions (constant amount of lipids separating two stripes), and the hexagonal packing of the gel-state lipids.

Among the diverse lipids occurring in biological membranes, there is usually a fraction that in the pure state would form a gel phase rather than the dominant lamellar liquid crystalline phase. There are also a few examples where a large fraction of the lipids have a melting temperature close to the body temperature, and the gel phase of the lipids can therefore play an important role. One example of this is the pulmonary lung surfactant, which is rich in DPPC. In fact, domains consisting of arrays of TM proteins have also been observed in pulmonary surfactant model systems (*6*). In the plasma membranes of eukaryotic cells, the gel-state-forming lipids are mainly associated with cholesterol in rafts in a liquid ordered state (*2, 4*). The accumulation and association of TM proteins in these domains is considered decisive for different biological functions.

REFERENCES

1. Rinia, H. A., Kik, R. A., Demel, R. A., Snel, M. M. E., Killian, J. A., van der Eerden, J., and de Kruijff, B. (2000) Visualization of highly ordered striated domains induced by transmembrane peptides in supported phosphatidylcholine bilayers, *Biochemistry 39*, 5852−5858.

2. Simons, K., and Ikonen, E. (1997) Functional rafts in cell membranes, *Nature 387*, 569−572.

3. Rinia, H. A., and de Kruijff, B. (2001) Imaging domains in model membranes with atomic force microscopy, *FEBS Lett. 504*, 194−199.

4. Brown, D. A., and London, E. (2000) Structure and function of sphingolipid- and cholesterol-rich membrane rafts, *J. Biol. Chem. 275*, 17221−17224.

5. Dufrene, Y. F., and Lee, G. U. (2000) Advances in the characterization of supported lipid films with the atomic force microscope, *Biochim. Biophys. Acta 1509*, 14−41.

6. Amrein, M., von Nahmen, A., and Sieber, M. (1997) A scanning force and fluorescence light microscopy study of the structure and function of a model pulmonary surfactant, *Eur. Biophys. J. 26*, 349−357.

7. Mou, J. X., Czajkowsky, D. M., and Shao, Z. F. (1996) Gramicidin A aggregation in supported gel state phosphatidylcholine bilayers, *Biochemistry 35*, 3222−3226.

8. Killian, J. A. (2003) Synthetic peptides as models for intrinsic membrane proteins, *FEBS Lett. 555*, 134−138.

9. Rinia, H. A., Boots, J. W. P., Rijkers, D. T. S., Kik, R. A., Snel, M. M. E., Demel, R. A., Killian, J. A., van der Eerden, J., and de Kruijff, B. (2002) Domain formation in phosphatidylcholine bilayers containing transmembrane peptides: Specific effects of flanking residues, *Biochemistry 41*, 2814−2824.

10. Fields, C. G., Lloyd, D. H., Macdonald, R. L., Otteson, K. M., and Noble, R. L. (1991) HBTU activation for automated Fmoc solid-phase peptide synthesis, *Peptide Res. 4*, 95−101.

11. White, P. (1992) in *Peptides, Chemistry, and Biology, Proc. 12th American Peptide Symposium* (Smith, J. A., and Rivier, J. E., Eds.) pp 537−538, ESCOM, Leiden, The Netherlands.

12. Knorr, R., Trzeciak, A., Bannwarth, W., and Gillesen, D. (1989) New coupling reagents in peptide synthesis, *Tetrahedron Lett. 30*, 1927−1930.

13. Ridder, A. N. J. A., Spelbrink, R. E. J., Demmers, J. A. A., Rijkers, D. T. S., Liskamp, R. M. J., Brunner, J., Heck, A. J. R., de Kruijff, B., and Killian, J. A. (2004) Photo-crosslinking analysis of preferential interactions between a transmembrane peptide and matching lipids, *Biochemistry 43*, 4482−4489.

14. Duff, D. G., Baiker, A., and Edwards, P. P. (1993) A new hydrosol of gold clusters 0.1. Formation and particle-size variation, *Langmuir 9*, 2301−2309.

15. de Planque, M. R. R., Kruijtzer, J. A. W., Liskamp, R. M. J., Marsh, D., Greathouse, D. V., Koeppe, R. E., de Kruijff, B., and Killian, J. A. (1999) Different membrane anchoring positions of tryptophan and lysine in synthetic transmembrane α-helical peptides, *J. Biol. Chem. 274*, 20839−20846.

16. Schägger, H., and von Jagow, G. (1987) Tricine-sodium dodecyl sulfate−polyacrylamide gel electrophoresis for the separation of proteins in the range from 1 to 100 kDa, *Anal. Biochem. 166*, 368−379.

17. Bollag, D. M., and Edelstein, S. J. (1991) *Protein Methods*, Wiley−Liss, New York.

18. Lakowicz, J. R. (1999) *Principles in Fluorescence Spectroscopy*, Kluwer Academic/Plenum Publishers, New York, pp 445−486.

19. Davis, J. H., Jeffrey, K. R., Bloom, M., Valic, M. I., and Higgs, T. P. (1976) Quadrupolar echo deuteron magnetic-resonance spectroscopy in ordered hydrocarbon chains, *ACS Symp. Ser.*, 70−77.

20. van Kan, E. J. M., Ganchev, D. N., Snel, M. M. E., Chupin, V., van der Bent, A., and de Kruijff, B. (2003) The peptide antibiotic clavanin A interacts strongly and specifically with lipid bilayers, *Biochemistry 42*, 11366−11372.

21. Duisenberg, A. J. M., Kroon-Batenburg, L. M. J., and Schreurs, A. M. M. (2003) An intensity evaluation method: EVAL-14, *J. Appl. Crystallogr. 36*, 220−229.

22. Rouser, G., Fleisher, S., and Yamamoto, A. (1970) Two-dimensional thin layer chromatographic separation of polar lipids and determination of phospholipids by phosphorus analysis of spots, *Lipids 5*, 494−496.

23. Brunner, J. (1996) Use of photocrosslinkers in cell biology, *Trends Cell Biol. 6*, 154−157.

24. Davis, J. H. (1983) The description of membrane lipid conformation, order and dynamics by ^{2}H-NMR, *Biochim. Biophys. Acta 737*, 117−171.

25. Tristram-Nagle, S., Zhang, R., Suter, R. M., Worthington, C. R., Sun, W. J., and Nagle, J. F. (1993) Measurement of chain tilt angle in fully hydrated bilayers of gel phase lecithins, *Biophys. J. 64*, 1097−1109.

26. Reithmeier, R. A. F. (1995) Characterization and modeling of membrane proteins using sequence analysis, *Curr. Opin. Struct. Biol. 5*, 491−500.

27. Rinia, H. A., Demel, R. A., van der Eerden, J., and de Kruijff, B. (1999) Blistering of Langmuir−Blodgett bilayers containing anionic phospholipids as observed by atomic force microscopy, *Biophys. J. 77*, 1683−1693.

28. Sansom, M. S. P. (1991) The biophysics of peptide models of ion channels, *Prog. Biophys. Mol. Biol. 55*, 139−235.

29. Copeland, B. R., and McConnell, H. M. (1980) The rippled structure in bilayer membranes of phosphatidylcholine and binary mixtures of phosphatidylcholine and cholesterol, *Biochim. Biophys. Acta 599*, 95−109.

30. Mortensen, K., Pfeiffer, W., Sackmann, E., and Knoll, W. (1988) Structural properties of a phosphatidylcholine-cholesterol system as studied by small-angle neutron-scattering—Ripple structure and phase diagram, *Biochim. Biophys. Acta 945*, 221−245.

31. Seul, M., and Andelman, D. (1995) Domain shapes and patterns: The phenomenology of modulated phases, *Science 267*, 476−483.

32. Morein, S., Killian, J. A., and Sperotto, M. M. (2002) Characterization of the thermotropic behavior and lateral organization of lipid−peptide mixtures by a combined experimental and theoretical approach: Effects of hydrophobic mismatch and role of flanking residues, *Biophys. J. 82*, 1405−1417.

33. Yano, Y., Takemoto, T., Kobayashi, S., Yasui, H., Sakurai, H., Ohashi, W., Niwa, M., Futaki, S., Sugiura, Y., and Matsuzaki, K. (2002) Topological stability and self-association of a completely hydrophobic model transmembrane helix in lipid bilayers, *Biochemistry 41*, 3073−3080.